Light Field Microscopy

Or how to make 4D snapshots

Gergo Bohner
Gatsby Tea Talk
11 Sept 2014

The Light Field

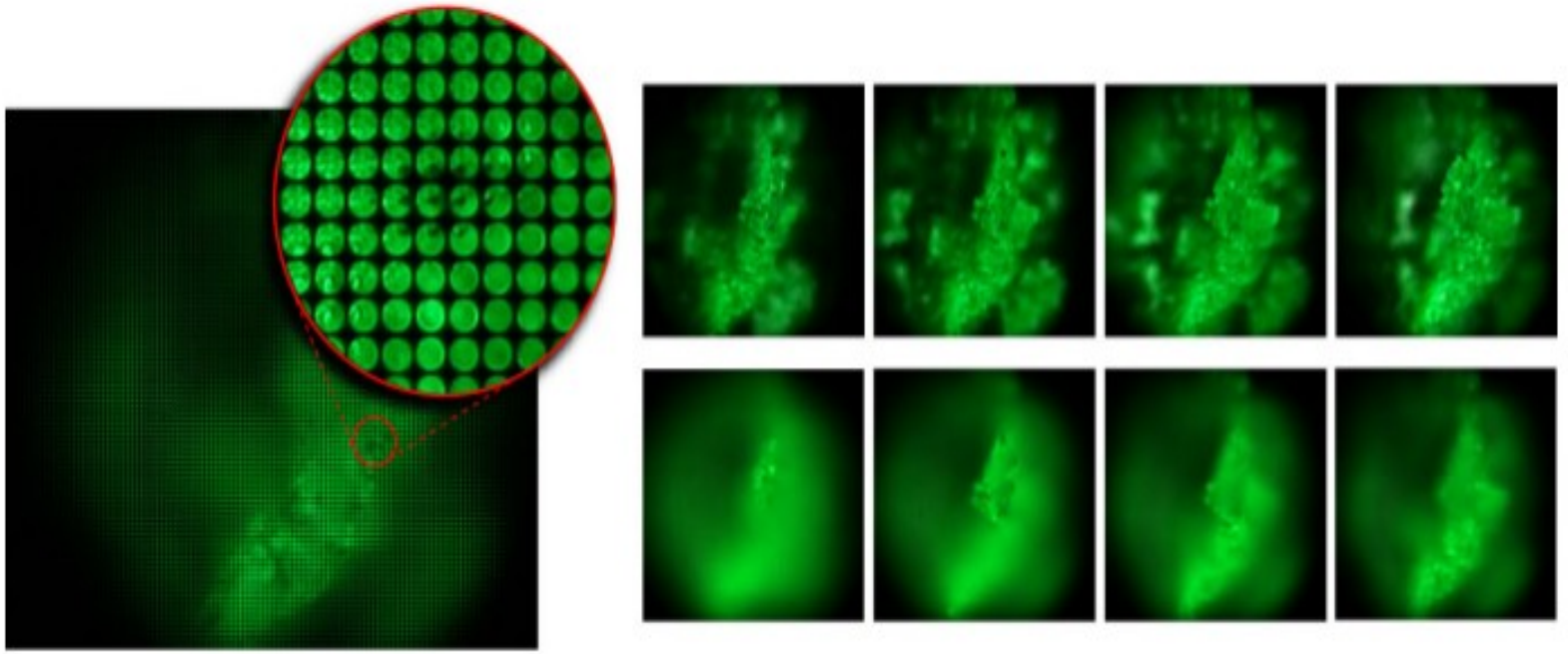

Figure 1: At left is a light field captured by photographing a speck of fluorescent crayon wax through a microscope objective and microlens array. The objective magnification is 16×, and the field of view is 1.3mm wide. The image consists of 170^2 subimages, one per microlens, each depicting a different part of the specimen. An individual subimage contains 20^2 pixels, each representing a different point on the objective lens and hence a unique direction of view. By extracting one pixel from each subimage, we can produce perspective views of the specimen, a sequence of which is shown at top-right. Alternatively, by summing the pixels in each subimage, we can produce orthographic views with a shallow depth of field, like an ordinary microscope but of lower spatial resolution. Shearing the light field before summing, we can focus at different depths, as shown in the sequence at bottom-right. These images were computed in real-time on a PC.

The Microscope

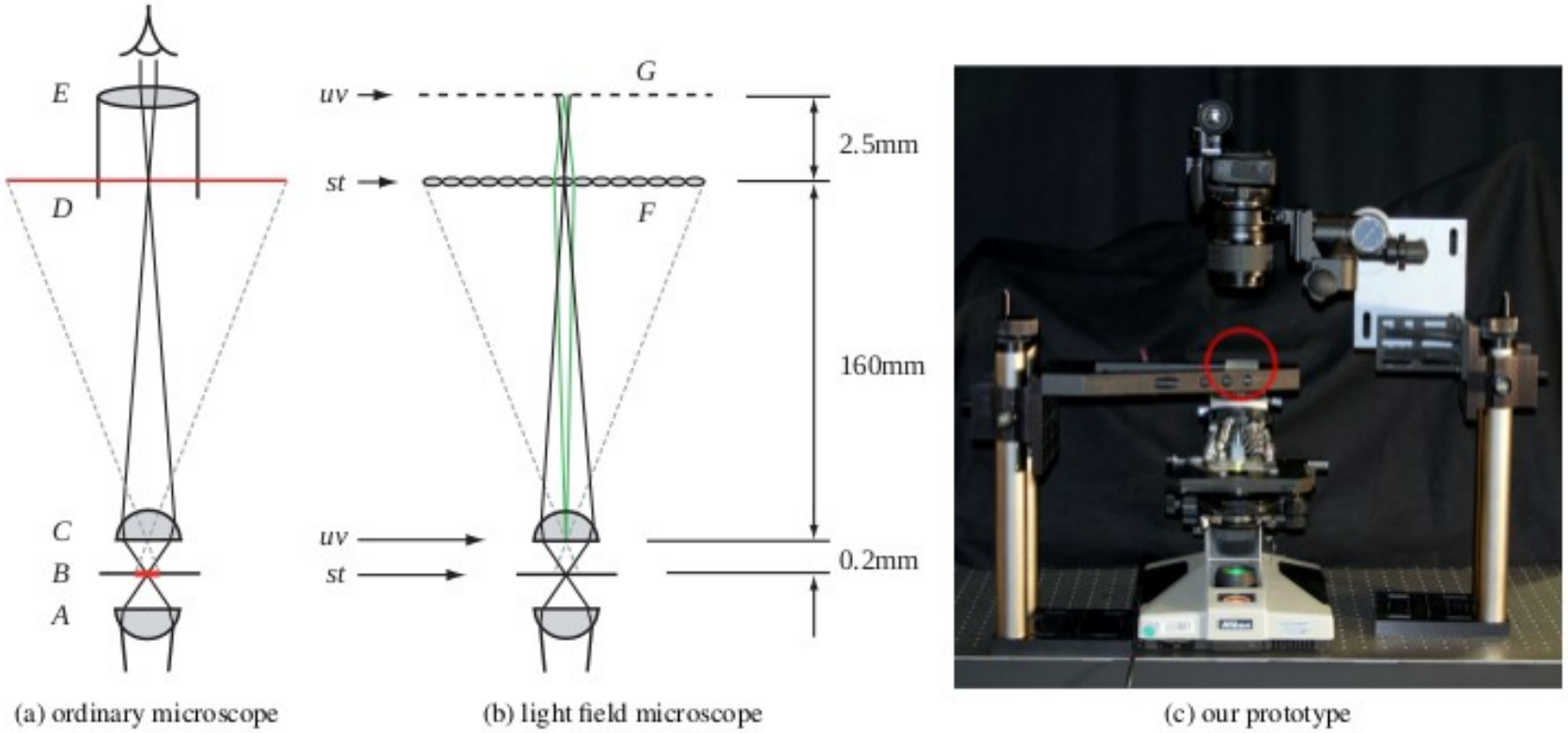

(a) ordinary microscope (b) light field microscope (c) our prototype

Figure 2: Optical layout of our light field microscope. (a) In a transmission-mode light microscope, an illumination source is focused by a condenser lens at *A* onto a specimen at *B*. An objective lens at *C* magnifies the specimen, creating a real image at intermediate image plane *D*. In older microscopes, this plane is located inside the microscope tube. An ocular (eyepiece) at *E* further magnifies the central portion of this image, creating a second image focused at infinity. (b) In our design the ocular is removed, a microlens array *F* is placed at the intermediate image plane, and a camera sensor is placed behind this at *G*, positioned so that each microlens records an in-focus image of the objective (green rays). In light field parlance, if the objective aperture and specimen constitute the *uv* and *st* planes, then the camera sensor and microlens array constitute a reimaging of these two planes. This drawing is not to scale; typical distances are shown beside it. (c) Our prototype consists of a Nikon Optiphot and custom microlens array (red circle). To avoid building a special camera, we re-image *G* using a Canon 5D 35mm SLR with a 1:1 macro lens.

The Microscope

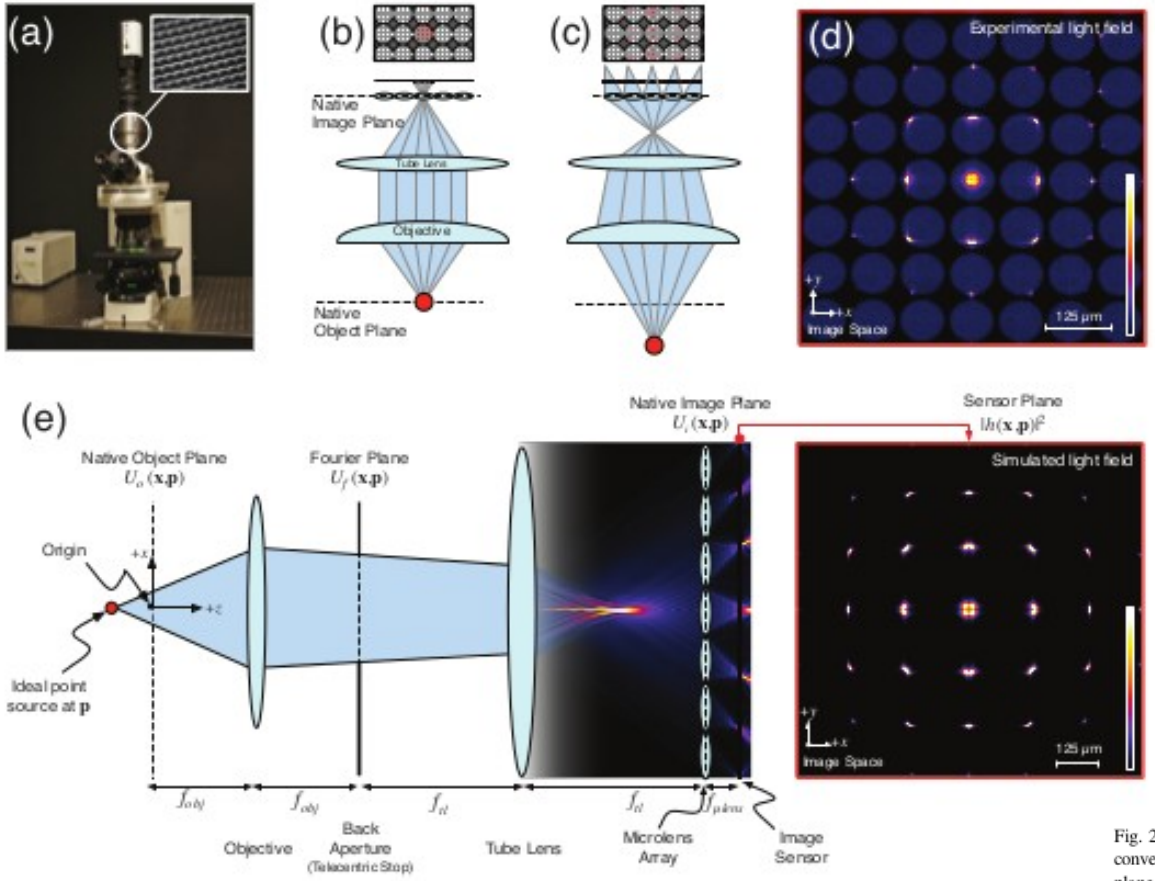

Fig. 2. Optical model of the light field microscope. **(a)** A fluorescence microscope can be converted into a light field microscope by placing a microlens array at the native image plane. **(b)** A ray-optics schematic indicating the pattern of illumination generated by one point source. The gray grid delineates pixel locations, and the white circles depict the back-aperture of the objective imaged onto the sensor by each lenslet. Red level indicates the intensity of illumination arriving at the sensor. For a point source on the native object plane (red dot), all rays pass through a single lenslet. **(c)** A point source below the native object plane generates a more complicated intensity pattern involving many lenslets. **(d)** A real light field recorded on our microscope using a 60x 1.4NA oil objective and a 125 µm pitch f/20 microlens array of a 0.5 µm fluorescent bead placed 4 µm below the native object plane. Diffraction effects are present in the images formed behind each lenslet. **(e)** A schematic of our wave optics model based on the LFM optical path (not drawn to scale). In this model, the microlens array at the native image plane is modeled as a tiled phase mask operating on this wavefront, which is then propagated to the camera sensor. The *xy* cross section on the far right shows the simulated light field generated at the sensor plane. The simulation is in good agreement with the experimentally measured light field in (d).

The Forward Model

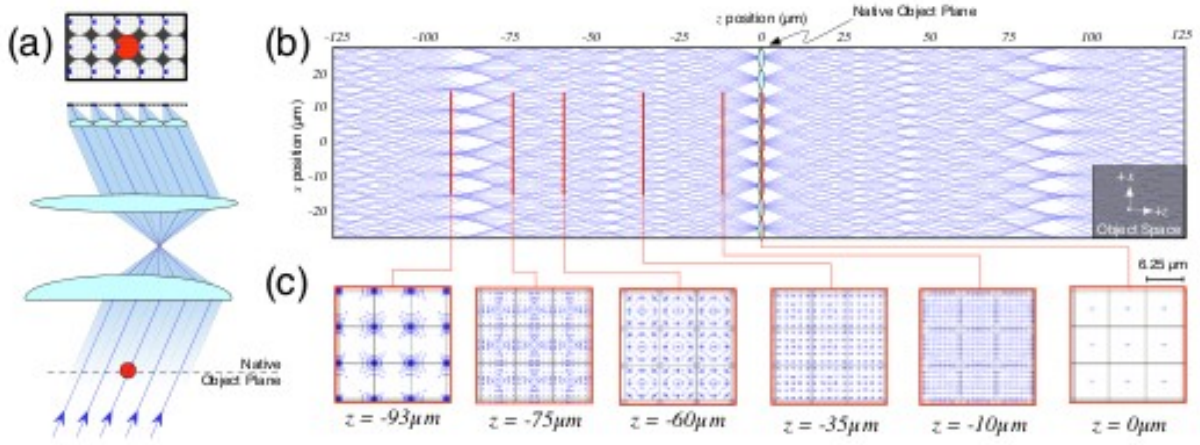

Fig. 3. Sampling of the volume recorded in a microlens-based light field. **(a)** A bundle of lenslet chief rays captured by the same pixel position relative to each lenslet (blue pixels) form a parallel projection through the volume, providing one of many angular views necessary to perform 3-D deconvolution. **(b)** When lenslet chief rays passing through every pixel in the light field are simultaneously projected back into the object volume, these rays cross at a diversity of x-positions (readers are encouraged to zoom into this figure in a PDF file to see how this pattern evolves with depth). This dense sampling pattern permits 3-D deconvolution with resolution finer than the lenslet spacing. The only place where this diversity does not occur is close to the native object plane; here resolution enhancement is not possible. **(c)** The distribution of the lenslet chief rays in xy cross-sections of the object volume changes at different distances from the native object plane. The outline of the lenslets are shown in light gray for scale. At $z = 0$ μm (rightmost image), the lack of spatial diversity in sample locations is evident.

The Deconvolution

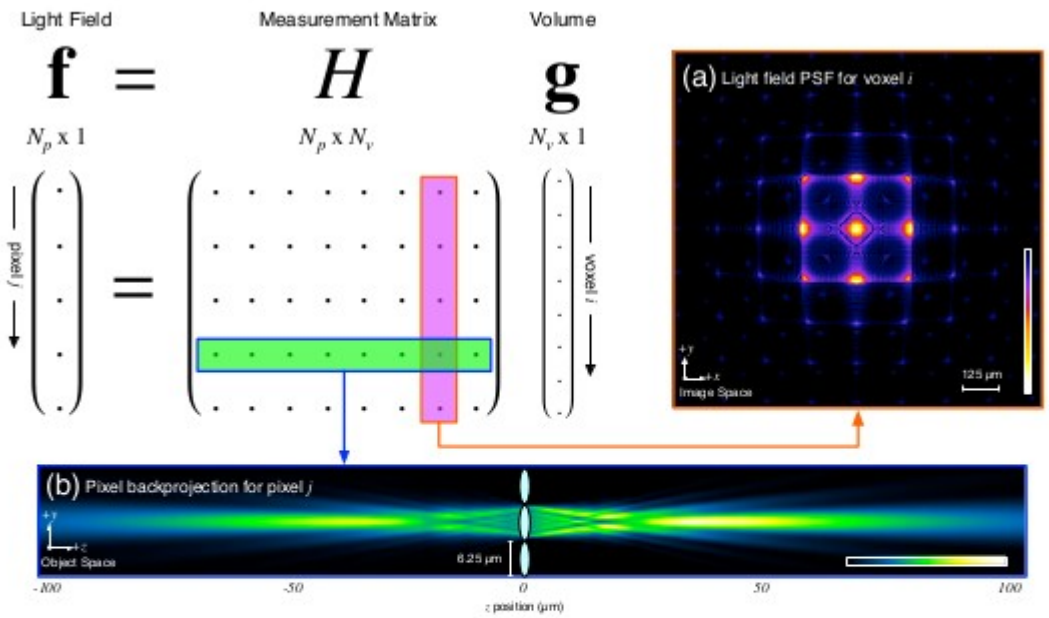

Fig. 4. The discrete light field imaging model, prior to accounting for sensor noise. The dimensionality of the light field **f** is fixed by the image sensor, but the dimensionality (or equivalently, the sampling rate) of the volume **g** is a user-selectable parameter in the reconstruction algorithm. **(a)** Column i of the measurement matrix H (purple) contains the discretized light field point spread function for voxel i, which corresponds to the forward projection of that point in the volume. **(b)** Row j of the measurement matrix (green) contains a pixel back projection: a visualization that shows how much each voxel in the volume contributes to a single pixel j in the light field. The cross sections in this figure were computed using our wave optics model for a 20x 0.5NA water dipping objective and a 125μm pitch f/20 microlens array.

$$\hat{\mathbf{f}} \sim \mathrm{Pois}(H\mathbf{g} + \mathbf{b}),$$

$$\Pr(\hat{\mathbf{f}}|\mathbf{g},\mathbf{b}) = \prod_i \left(\frac{(H\mathbf{g}+\mathbf{b})_i^{\hat{\mathbf{f}}_i} \exp(-(H\mathbf{g}+\mathbf{b})_i)}{\hat{\mathbf{f}}_i!} \right),$$

Ricardson-Lucy iterative deconvolution

$$\mathbf{g}^{(k+1)} = \mathrm{diag}(H^T\mathbf{1})^{-1}\,\mathrm{diag}(H^T\,\mathrm{diag}(H\,\mathbf{g}^{(k)} + \mathbf{b})^{-1}\mathbf{f})\,\mathbf{g}^{(k)},$$

Resolution

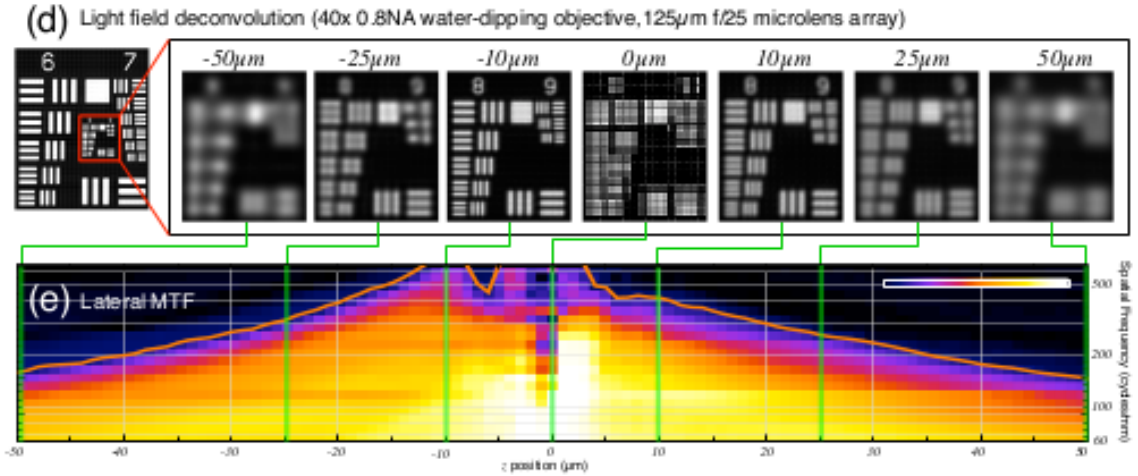

Fig. 5. Experimentally characterized resolution limits for two optical configurations of the light field microscope. **(a)** In a widefield microscope with no lenslet array, the target quickly goes out of focus when it is translated in z. **(b)** In a 3-D deconvolution from a light field, we lose resolution if the test target is placed at the native object plane ($z = 0$ μm), but we can reconstruct the target at much higher resolution than the spacing between lenslets when it is moved $z = -15$ μm (see also Fig. 1). Resolution falls off gradually beyond this depth ($z = \pm 50$ μm and ± 100 μm). **(c)** Experimental MTF measured by analyzing the contrast of different line pair groupings in the USAF reconstruction. The colormap shows normalized contrast as measured using Eq. (10). The region of fluctuating resolution from $z = -30$ μm to 30 μm show that not all spatial frequencies are equally well reconstructed at all depths. **(d)** A slightly higher peak resolution ($z = \pm 10$ μm) can be achieved in the light field recorded with a 40x 0.8NA objective. However, the $z = \pm 25$ μm and ± 50 μm planes in (d) have the same apparent resolution as the $z = \pm 50$ μm and ± 100 μm planes in (b). **(e)** The experimental MTF for the 40x configuration shows that the region of fluctuating resolution (from -7.5 μm to 7.5 μm) is one quarter the size compared to (c). The solid green line in (c) and orange line in (e) are a 10% contrast cut-off representing the band limit of the reconstruction as a function of depth. Note that these plots are clipped to 645 cycles/mm, which is the highest resolution group on the USAF target.

Results

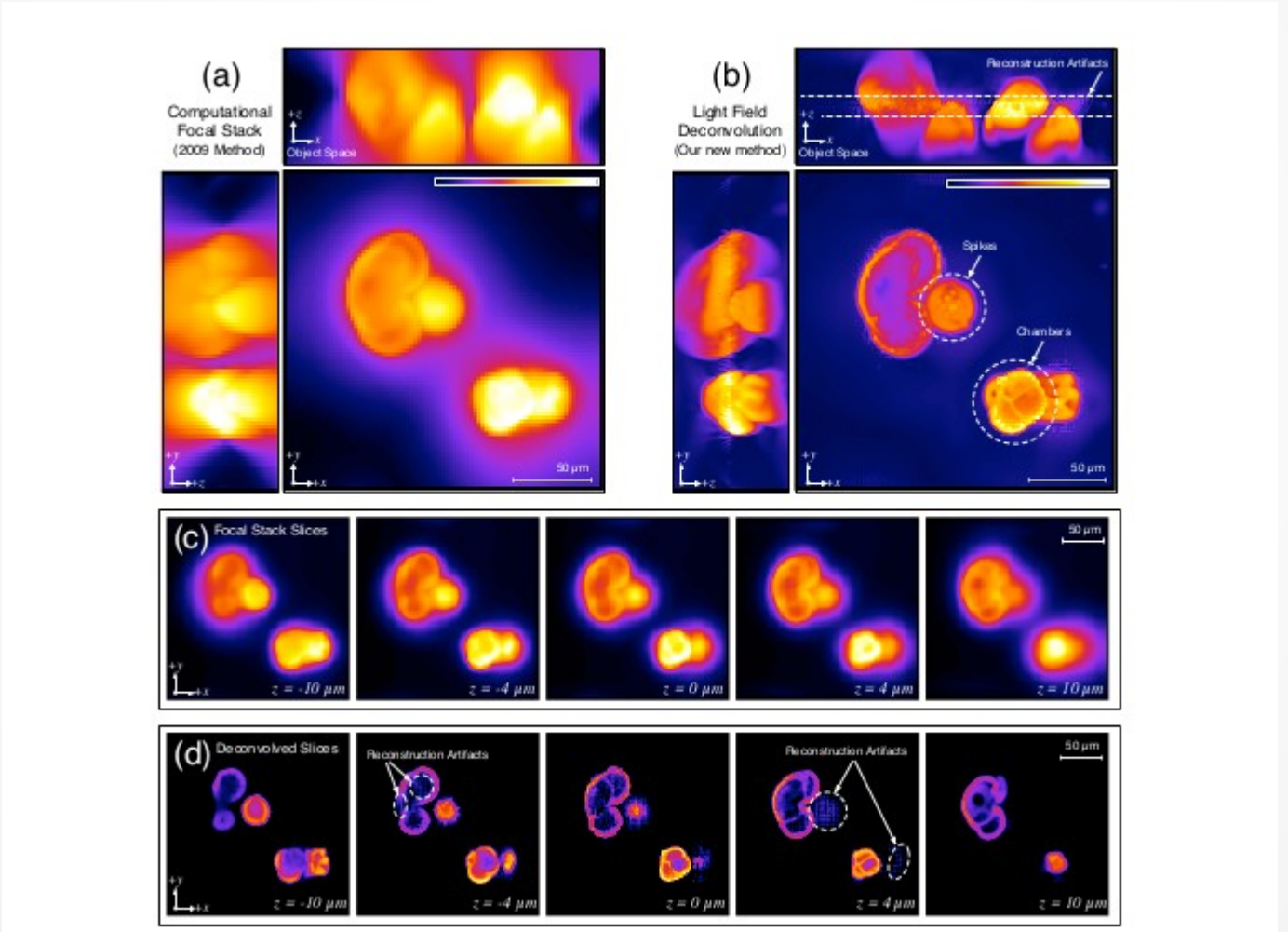
(a)
Computational
Focal Stack
(2009 Method)
Object Space
50 µm
(b)
Light Field
Deconvolution
(Our new method)
Reconstruction Artifacts
Object Space
Spikes
Chambers
50 µm
(c) Focal Stack Slices
z = -10 µm
z = -4 µm
z = 0 µm
z = 4 µm
z = 10 µm
50 µm
(d) Deconvolved Slices
Reconstruction Artifacts
Reconstruction Artifacts
z = -10 µm
z = -4 µm
z = 0 µm
z = 4 µm
z = 10 µm
50 µm

Results

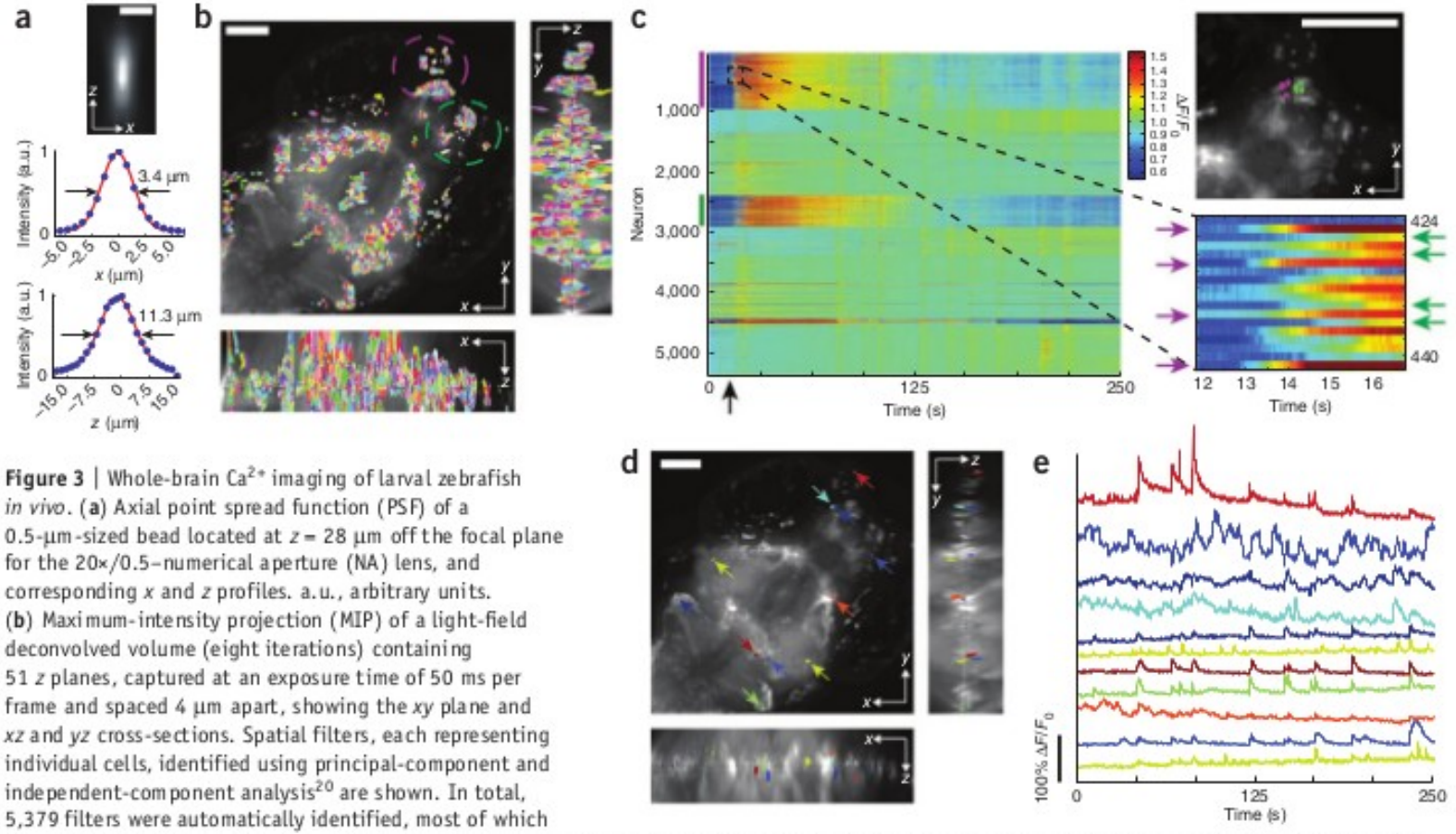

Figure 3 | Whole-brain Ca^{2+} imaging of larval zebrafish *in vivo*. (**a**) Axial point spread function (PSF) of a 0.5-µm-sized bead located at $z = 28$ µm off the focal plane for the 20×/0.5–numerical aperture (NA) lens, and corresponding x and z profiles. a.u., arbitrary units. (**b**) Maximum-intensity projection (MIP) of a light-field deconvolved volume (eight iterations) containing 51 z planes, captured at an exposure time of 50 ms per frame and spaced 4 µm apart, showing the xy plane and xz and yz cross-sections. Spatial filters, each representing individual cells, identified using principal-component and independent-component analysis[20] are shown. In total, 5,379 filters were automatically identified, most of which correspond to individual neurons. (**c**) Extracted Ca^{2+} intensity signal ($\Delta F/F_0$) of GCaMP5 fluorescence using spatial filters shown in **b**. Each row shows a time-series heat map. Color bars denote encircled regions in **b**, which include the olfactory epithelium, olfactory bulb and telencephalon. The arrow at ~15 s denotes the addition of an aversive odor. A close-up of the dashed box is shown (right, lower panel); neurons with subtle differences in response onset are highlighted by colored arrows. The location of these neurons in the MIP is also shown (right, upper panel). (**d**) Overlay of the MIP with randomly selected spatial filters (colored dots and arrows). (**e**) Ca^{2+} intensity traces of selected cells shown in **d**. Neurons were manually selected from the olfactory system, midbrain and hindbrain. Trace color matches spatial-filter color in **d**. Also see **Supplementary Video 6**. Scale bars, 10 µm (**a**) and 100 µm **b**–**d**.

Results

Discussion

- Basic light field microscopes are easy to build and use
- Offline high quality deconvolution is possible via extremely complicated forward model
- Via beam-splitters one can achieve high resolution in all axial planes
- Can achieve high temporal resolution (50 Hz) on whole zebrafish larvae, bit useless with current Ca^{2+} indicators

References

- Light Field Microscopy, Levoy et al, 2006, Proceedings of ACM
- Wave optics theory and 3-D deconvolution for the light field microscope, Broxton et al, 2013, Optics Express
- Simultaneous whole-animal 3D imaging of neuronal activity using light-field microscopy, Prevedel et al, 2014, Nature methods